NASA Technical Memorandum 79280

EXPERIMENTAL STUDY OF LOW ASPECT RATIO COMPRESSOR BLADING

Lonnie Reid and Royce D. Moore
Lewis Research Center
Cleveland, Ohio

Prepared for the
Twenty-fifth Annual International Gas Turbine Conference
sponsored by the American Society of Mechanical Engineers
New Orleans, Louisiana, March 9-13, 1980

NOMENCLATURE

D	diffusion factor
i_{ss}	suction surface incidence angle, angle between inlet air direction and line tangent to blade suction surface at the leading edge, deg
K_{ss}	angle between a line tangent to blade suction surface and meridional direction, deg
M	Mach number
P	total pressure, N/cm^2
p	static pressure, N/cm^2
r	spanwise radius in meridional plane, cm
T	total temperature, K
W	mass flow, kg/sec
V	air velocity, m/sec
β	air angle, angle between air velocity and meridional direction, deg
β'_c	relative meridional flow angle based on cone angle, deg
γ	ratio of specific heats, 1.40
δ	ratio of pressure to standard day pressure
η	efficiency
θ	ratio of total temperature to standard day temperature
σ	solidity, ratio of chord to blade spacing
$\overline{\omega}$	total loss coefficient
$\overline{\omega}_p$	total loss parameter

SUBSCRIPTS

ad	adiabatic
id	ideal
le	leading edge
te	trailing edge
θ	tangential direction
1	instrument station upstream of rotor
2	calculation station downstream of rotor
3	instrument station downstream of stator

SUPERSCRIPT

'	relative to blade

INTRODUCTION

The attainment of improved cycle efficiency for advanced gas turbine engines requires increased pressure ratio for the core compressor. During the past few years NASA Lewis has been conducting an extensive research program on axial flow compressors with high pressure ratio transonic stages. As a part of this program, four single-stage compressors, that are representative of the inlet stage of a multistage core compressor, were designed and evaluated experimentally.

The stage designs feature two levels of rotor aspect ratio (1.19 and 1.63) and two levels of pressure ratio (1.82

and 2.05). The aerodynamic designs as well as the comparisons of overall performance data for the four stages are given in reference 1. This paper presents a more detailed investigation of the flow phenomena for the four stages utilizing selected blade element parameters. Comparisons of blade element parameters are presented for the two different aspect ratio configurations at each of the design pressure ratio levels. Blade loading levels (diffusion factors) are compared for the near-stall conditions at all speeds tested. Comparisons are made of loss and diffusion factors (D-factors) over the operating range of incidence angles at several span locations. The axial distributions of rotor tip static pressure are presented for three flow conditions at design speed for all four stages.

APPARATUS AND PROCEDURE

Test Facility

The compressor stages were tested in the Lewis Research Center single stage compressor test facility, which is described in detail in reference 2. A schematic diagram of the facility is shown in figure 1. Atmospheric air enters the facility at an inlet located on the roof of the building and flows through the flow-measuring orifice and into the plenum chamber upstream of the test stage. The air then passes through the experimental compressor stage into the collector and is exhausted to the atmospheric exhaust system. The rotor is driven by a variable-speed electric motor through a gearbox.

Test Compressors

The detailed aerodynamic and mechanical designs of the compressors used in this investigation are presented in reference 1 and thus only a brief description will be presented herein. The basic designs feature two levels of stage pressure ratio, two levels of rotor aspect ratio, and two levels of stator aspect ratio. The designs are summarized in table I. Stages 35 and 36, having a design pressure ratio of 1.82 were designed for rotor blade aspect ratios of 1.19 and 1.63, respectively. Similarly, stages 37 and 38, having a design pressure ratio of 2.05, also had rotor blade aspect ratios of 1.19 and 1.63, respectively. Stator vane aspect ratios were 1.26 and 1.78. All of the rotor and stator blades have multiple circular arc airfoils. Careful positioning of the blade rows allowed all four stages to be tested with the same flow path geometry (fig. 2). The design specific flow (100.1 kg/sec/cm^2) and rotor tip speed (455.0 m/sec) were the same for all four stages. These are relatively high values of mass flow and tip speed for core type stages.

Test Procedure

The stage survey data were taken over a range of flows for speeds from 50 to 100 percent of design speed. For each flow, data were recorded at nine radial positions upstream (station 1) and downstream (station 3) of the test stage. At station 3, the instrumentation was also circumferentially traversed to nine positions across the stator gap. The axial locations of the survey stations are shown in figure 2. The survey measurements consisted of total pressure, static pressure, total temperature, and flow angle. Flow was measured with a thin plate orifice. A more complete description of the survey instrumentation and test procedure is given in reference 1.

The estimated errors in the data, based on inherent accuracies of the instrumentation and recording system, are as follows:

Flow, kg/sec	±0.3
Rotative speed, rpm	±30
Flow angle, deg	±1.0
Temperature, K	±0.6
Rotor-inlet (station 1) total pressure, N/cm^2	±0.01
Rotor-inlet (station 1) static pressure, N/cm^2	±0.03
Stator-outlet (station 3) total pressure, N/cm^2	±0.17
Stator-outlet (station 3) static pressure, N/cm^2	±0.10

Calculation Procedure

Because of the close spacing between the rotor and stator, no instrumentation could be used at station 2 (see fig. 2). The values of pressure, temperature, and flow angle at this station were obtained as follows: At each radial survey position, total pressure and total temperature were translated along design streamline from station 3. The circumferentially mass-averaged total temperatures from station 3 were used as the total temperatures at station 2. The arithmetic mean of the three highest total pressure values from the circumferential distributions at station 3 were used as the total pressures at station 2. The radial distributions of static pressure and flow angle were calculated based on continuity of mass flow and radial equilibrium. Measured airflow and rotative speed were inputs. Design values of streamline curvature and blockages were also used in the calculations.

All data are corrected to standard day conditions based on the rotor inlet conditions. Overall total pressure ratios and total temperature ratios are based on an energy average of the pressures and temperatures obtained from the calibrated survey instrumentation. Blade element data are translated along design streamlines to the blade leading and trailing edges. Details of the calculation procedure are given in reference 1.

RESULTS AND DISCUSSION

An assessment of the effects of blade aspect ratio is made by comparing some of the basic flow phenomenon for the two aspect ratio configurations for each level of design pressure ratio. The overall performance comparisons are presented to show the overall effects of blade aspect ratio on the performance characteristics. Radial distributions of performance parameters are compared for the peak efficiency conditions at design speed to show how the difference

in overall performance manifests itself over the blade span. Rotor tip and stator hub diffusion factors for the four stages are compared for the near-stall conditions over the entire speed range. This comparison is made in an attempt to determine which blade row is controlling the flow range and to assess the effects of blade aspect ratio on blade loading limits. Blade element performance comparisons are made to assess the effects of blade aspect ratio on typical blade element parameters over a range of flow conditions. Axial distribution of rotor tip static pressures are presented at design speed to assess the effect of blade aspect ratio on end wall flow conditions when shocks are present.

Overall Performance Comparisons

The effects of aspect ratio on overall performance are presented in figure 3. For both design pressure ratio levels, the overall rotor and stage performances for the lower aspect ratio configurations are substantially better than those for the higher aspect ratio configurations. The lower aspect ratio configurations achieved a higher peak pressure ratio and efficiency and a larger flow range over the range of speeds tested. The largest increase in flow range occurred at the design speed.

For the higher design pressure ratio configurations the peak rotor efficiency, at design speed, for the lower aspect ratio configuration (stage 37) is about 2.5 points higher than that for the higher aspect ratio configuration (fig. 3(a)). However, the difference in stage efficiency is about one point.

Similar trends are shown for the lower design pressure ratio configurations (fig. 3(b)). At design speed, the peak efficiency for both rotor and stage is approximately 2 points higher for the lower aspect ratio configuration.

The highest overall rotor and stage efficiencies were obtained with the lower aspect ratio higher-pressure configuration (stage 37) and they occurred at 90 percent design speed. The maximum rotor and stage efficiencies are 91.6 percent and 89.3 percent, respectively. The corresponding pressure ratios are 1.775 and 1.751.

The peak efficiencies at design speed along with the corresponding pressure ratios for rotor and stage for all four configurations are summarized in table II. Also shown are the values of stall margin based on conditions at peak efficiency and stall.

Radial Distributions of Performance Parameters

Comparisons of the radial distributions of rotor performance parameters, for the peak rotor efficiency at design speed, are presented in figure 4. Some general trends, common to both aspect ratio configurations, are noted. The radial distributions of total pressure ratio are similar for all four rotors. The highest pressure ratio and efficiency occurred in the hub region. For both levels of design pressure ratio, the lower aspect ratio rotors (35 and 37) achieved higher efficiencies and higher pressure ration over practically the entire blade span. The radial distribution of rotor inlet relative Mach number is practically identical for all four configurations. The rotor inlet relative Mach numbers are supersonic over the entire span and the exit relative Mach numbers (not shown) are subsonic over the entire blade span. It is apparent that the distributions of efficiency and total loss parameters are strongly influenced by the shock losses.

In comparing the lower design pressure ratio configurations (fig. 4(a)), the efficiency difference is most pronounced in the region from 30 to 85 percent span. There is a noticeable inflection in the efficiency distributions at the 50-percent span location for both rotors. This could be a result of large shock losses associated with the high inlet relative Mach (1.4) and high blade loading for this spanwise location. For the lower aspect ratio rotor (rotor 35), the efficiency varies from about 0.80 in the tip region to 0.927 at the 85-percent span location. For the higher aspect ratio rotor (rotor 36), the efficiency varies from about 0.79 in the tip region to 0.902 at the 85-percent span location. In comparing the higher design pressure ratio rotors (rotors 37 and 38), the efficiency for the lower aspect ratio rotor (rotor 37) varies from about 0.77 in the tip region to 0.938 at the 85-percent span location. For the higher aspect ratio rotor, the efficiency varies from 0.76 in the tip region to 0.904 at the 85-percent span location.

Effects of Aspect Ratio on Stall D-Factor

Although the diffusion factor (D-factor) was developed to represent blade loading in a flow field that is totally subsonic, it is commonly used to correlate data from blade rows that operate in a transonic flow field. For flows with shocks, it is recognized that the diffusion factor is questionable for expressing local diffusion (blade loading) on the blade surfaces. However, D-factor has been used with some success in correlating losses and stall margin for transonic blade rows. This indicates that comparative results utilizing D-factor correlations for transonic blade rows can be useful when applied in a consistent manner. This section shows, on a relative basis, how the D-factors for the near-stall conditions vary with blade aspect ratio.

The diffusion factor and inlet relative Mach number are plotted in figure 5 as a function of percent design speed at the near-stall condition for all four stages. Data are shown for the rotor tip (10% span) and stator hub (90% span). Considering that the rotor tip diffusion factors are substantially higher than the corresponding stator hub diffusion factors and that the maximum stator hub Mach number is about 0.83, it is reasonable to assume that the flow range is limited by the flow conditions in the rotor tip region for all four stages. For the rotor tip (fig. 5(a)), the inlet relative Mach numbers at the near-stall conditions are practically the same for all four rotors. However, the rotor diffusion factors at the near-stall conditions show that the stalling D-factors are substantially larger for the lower aspect ratio

rotors (rotors 35 and 37) than those for the higher aspect ratio configurations at all speeds with a possible exception of the 50-percent speed. For all rotors, the largest value of diffusion factor at near-stall conditions occurred at design speed. The higher design pressure ratio low aspect ratio rotor (rotor 37) had the highest stall diffusion factor of 0.645. This value of diffusion factor is higher than that for other inhouse higher aspect ratio rotors with comparable inlet relative Mach numbers.

The diffusion factor and inlet Mach number at the stator hub (90% span from tip) are plotted as a function of design speed in figure 5(b). The trends of Mach number and D-factor variations with percent design speed are similar to those for the rotor. However, the diffusion factor values are not considered to be stall values for these stators. It is of interest to note, however, that at an inlet Mach number of approximately 0.83 stator 37 (lower aspect ratio) operated at a diffusion factor of approximately 0.575. Based on NASA experience, this is an unusually high value of stator hub diffusion factor for this level of inlet Mach number.

Blade Element Performance Comparisons

Comparisons of rotor blade element performance parameters for the high and low aspect ratio configurations and for each level of design pressure ratio are presented in figure 6. Data are presented for the 10-, 50-, and 90-percent span locations at design speed. Total loss parameter and diffusion factor are plotted as a function of suction surface incidence angles. The lower aspect ratio rotors operated over a wide range of incidence angles than the higher aspect ratio rotors for all three blade elements. For the lower aspect ratio rotors, the 10- and 50-percent elements operated to higher diffusion factors levels than the higher aspect ratio rotors. For the 10- and 50-percent span, the blade elements for the low and high aspect ratio rotors operated along the same incidence angle loss characteristics.

Axial Distributions of Rotor Tip Static Pressure

For rotor blade rows operating in a transonic flow environment, the axial distribution of the time-averaged static pressures over the rotor tips is strongly influenced by the shock patterns within the blade passage. In an attempt to qualitatively relate these axial distributions of static pressure to the shock patterns within the blade, data from another transonic rotor are presented (ref. 3). These data include both the axial distributions of rotor tip static pressures and shock patterns within the blade passage. The shock patterns were obtained from intrablade flow field measurements made with a Laser Anemomenter (LA) system. The blade passage shock patterns along with the axial distributions of rotor tip static pressure are presented in figure 7 for the maximum flow and near-stall conditions. The shock patterns derived from the LA system measurements are for the 15-percent span (from the tip) location. The axial distributions of static pressures measured on the casing over the rotor tips are ratioed to rotor inlet total pressure and plotted as a function of percent of rotor projected chord. At the maximum flow condition (fig. 7(a)), there is a weak shock at the blade entrance region and a strong shock at the exit of the blade passage. The static pressure gradients in the front and rear portions of the blades are indicative of these passage shock strengths. For the near-stall condition (fig. 7(b)) there is a strong passage shock at the blade entrance region. The strength of the shock is represented by the steep static pressure gradient in the front portion of the blade. However, just downstream of the shock the gradient decreases. These data provide a qualitative assessment of how the axial distribution of time-averaged rotor tip static pressure is influenced by the shock patterns within the blade passage. Based on this assessment the shock strengths will be inferred from the axial distributions of rotor tip static pressure for the rotors evaluated in the low aspect ratio study.

The axial distributions of rotor tip static pressure are presented in figure 8 for all four rotor configurations. Data are presented at design speed for three flow rates; maximum flow, peak efficiency, and near-stall conditions. These curves (fig. 8) show quite similar static pressure gradients for rotors with the same aspect ratio even though the blade rows are designed for different total pressure ratios. This implies that the shock patterns for the low aspect ratio rotors (rotors 35 and 37) are similar and the shock patterns for the higher aspect ratio rotors (rotors 36 and 38) are similar.

For the lower aspect ratio rotors, as the back pressure is increased (lower flow), there is a substantial increase in the static pressure gradient over the front portion of the blade. This indicates that the strength of the shock is increasing and the shock is moving forward in the blade passage. The smooth and continuous static pressure rise on the rear portion of the blade indicates good subsonic diffusion even behind a strong shock.

For the higher aspect ratio rotors, as the back pressure is increased (lower flow), the increase in static pressure gradient over the front portion of the blade is small. However, the static pressure gradients in the 50- to 60-percent chord region increases very rapidly, and then drops off substantially just downstream of the 60-percent chord location. This indicates a strong shock and poor diffusion caused by flow separation and recirculation just downstream of the shock.

A comparison of the axial distribution of rotor tip static pressures for the near-stall conditions is presented in figure 9 for the low and high aspect ratio configurations. The comparison shows that the higher aspect ratio rotors have steeper static pressure gradients than the lower aspect ratio configurations. This indicates that it is the

steeper static pressure gradient, caused by the shock patterns, that is responsible for the relative poor flow range for the higher aspect ratio configurations.

REMARKS

Benefits of lower aspect ratio blading for achieving good efficiency at higher loading levels have generally been demonstrated with stages designed for subsonic flows. In this study the application of low aspect ratio blading to rotors with high loading and high supersonic inlet relative Mach numbers over the entire blade span was investigated. The good efficiency and relatively higher flow range achieved with the lower aspect ratio configuration demonstrates that low aspect ratio blading is highly beneficial for transonic blade rows. For advanced high pressure multistage core compressor the inlet stages must operate at high loading level and high inlet relative Mach numbers. There has been a question whether sufficient flow range can be obtained with stages of this type such that they would be suitable for multistage application. Results of this study indicate that through the use of low aspect ratio blading, high Mach number, highly loaded stages can achieve a performance level suitable for multistage compressor applications.

SUMMARY OF RESULTS

This paper presents a study of low aspect blading for inlet stages of a high pressure ratio, high-speed core compressor. The basic overall design variables were stage pressure ratio and blade aspect ratio. These four stages represent two levels of total pressure ratio (1.82 and 2.05), two levels of rotor blade aspect ratio (1.19 and 1.63) and two levels of stator vane aspect ratios (1.26 and 1.78). Comparisons of overall performance, radial distributions of performance parameters, diffusion factors at the near-stall conditions, blade element data, and axial distribution of rotor tip static pressures has yielded the following results:

1. Higher peak pressure ratio, high stage and rotor effiencicies and greater stall margin were obtained with the lower aspect ratio blading.
2. The lower aspect ratio blading showed improved performance over the entire blade span.
3. The lower aspect ratio rotors operated at higher diffusion factors and higher incidence angles over the entire blade span.
4. Better subsonic diffusion downstream of the passage shock was obtained in the lower apsect ratio rotors.

APPENDIX - EQUATIONS

Suction surface incidence angle:

$$i_{ss} = \left(\beta'_c\right)_{le} - \left(K_{ss}\right)_{le}$$

Diffusion factor:

$$D = 1 + \frac{V'_{te}}{V'_{le}} + \left| \frac{\left(rV_\theta\right)_{te} - \left(rV_\theta\right)_{le}}{\left(r_{te} + r_{le}\right)\left(V_i\right)_{le}} \right|$$

Total loss coefficient:

$$\overline{\omega} = \frac{\left(P'_{id}\right)_{te} - (P')_{te}}{(P')_{le} - (P)_{le}}$$

Total loss parameter:

$$\overline{\omega}_p = \frac{\overline{\omega} \cos (\beta')_{te}}{2\sigma}$$

Adiabatic efficiency:

$$\eta_{ad} = \frac{\left[\frac{(P)_{te}}{(P)_{le}}\right]^{\gamma-1/\gamma} - 1}{\frac{(T)_{te}}{(T)_{le}} - 1}$$

Equivalent mass flow:

$$\frac{W\sqrt{\theta}}{\delta}$$

Stall margin:

$$SM = \left[\frac{\left(P_3/P_1\right)_{stall} \left(\frac{W\sqrt{\theta}}{\delta}\right)_{ref}}{\left(P_3/P_1\right)_{ref} \left(\frac{W\sqrt{\theta}}{\delta}\right)_{stall}} - 1 \right] \times 100$$

REFERENCES

1. Reid, L., and Moore, R. D., "Design and Overall Performance of Four Highly Loaded, High-Speed Inlet Stages for an Advanced High-Pressure-Ratio Core Compressor," NASA TP-1337, 1978.
2. Urasek, D. C., and Janetzke, D. C., "Performance of Tandem-Bladed Transonic Compressor Rotor with Rotor Tip Speed of 1375 Feet Per Second," NASA TM X-2484, 1972.
3. Powell, A. J., Strazisar, C. J., and Seasholtz, R. G., "Efficient Laser Anemometer for Intrarotor Flow Mapping in Turbomachinery," Paper to be presented at the conference.

TABLE I. - DESIGN OVERALL PERFORMANCE PARAMETERS FOR STAGES 35, 36, 37, AND 38

Parameters	Stage			
	35	36	37	38
Rotor total pressure ratio	1.865	1.863	2.106	2.105
Stage total pressure ratio	1.820	1.820	2.050	2.050
Rotor total temperature ratio	1.225	1.227	1.270	1.269
Stage total temperature ratio	1.225	1.227	1.270	1.269
Rotor adiabatic efficiency	0.865	0.858	0.877	0.878
Stage adiabatic efficiency	0.828	0.822	0.842	0.844
Rotor polytropic efficiency	0.877	0.870	0.889	0.890
Stage polytropic efficiency	0.842	0.837	0.857	0.859
Rotor head rise coefficient	0.273	0.272	0.333	0.331
Stage head rise coefficient	0.262	0.261	0.319	0.318
Flow coefficient	0.451	0.447	0.453	0.448
Weight flow per unit frontal area	100.808	100.464	100.950	100.525
Weight flow per unit annulus area	199.989	198.640	200.549	198.877
Weight flow	20.188	20.188	20.188	20.188
RPW	17 188.700	17 188.700	17 185.700	17 188.700
Tip speed	454.456	455.233	454.136	455.096
Hub-tip radius ratio	0.70	0.70	0.70	0.70
Rotor aspect ratio	1.19	1.63	1.19	1.63
Stator aspect ratio	1.26	1.78	1.26	1.77
Number of rotor blades	36.6	48.0	36.0	48.0
Number of stator blades	46.0	62.0	46.0	62.0

TABLE II. - SUMMARY OF OVERALL PERFORMANCE

Stage number	Rotor aspect ratio	Rotor peak efficiency	Stage peak efficiency	Rotor pressure ratio	Stage pressure ratio	Stall margin
37	1.19	0.876	0.840	2.056	2.000	10
35	1.19	.872	.845	1.875	1.842	21
36	1.63	.852	.821	1.766	1.730	11
38	1.63	.849	.831	1.969	1.944	0

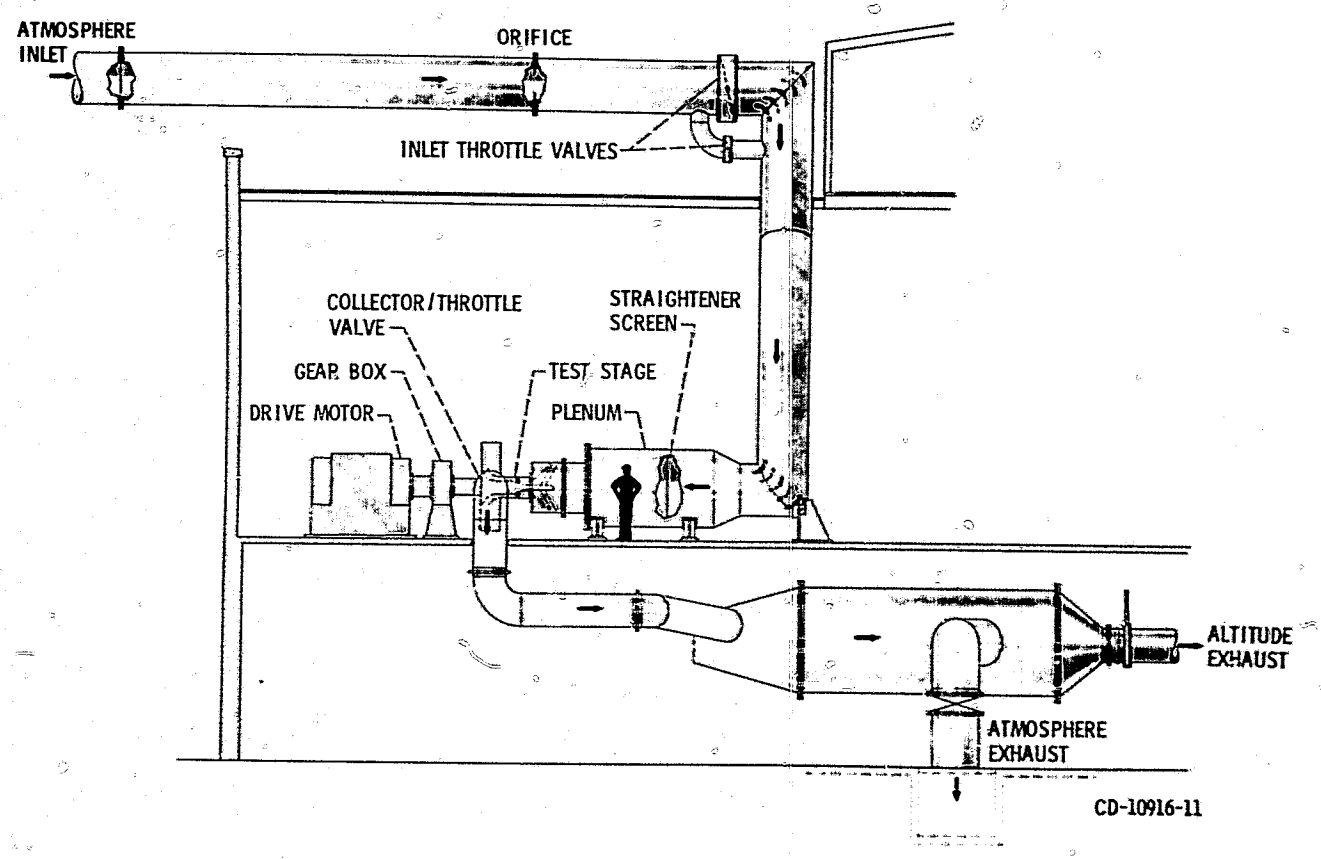

Figure 1. - Compressor test facility.

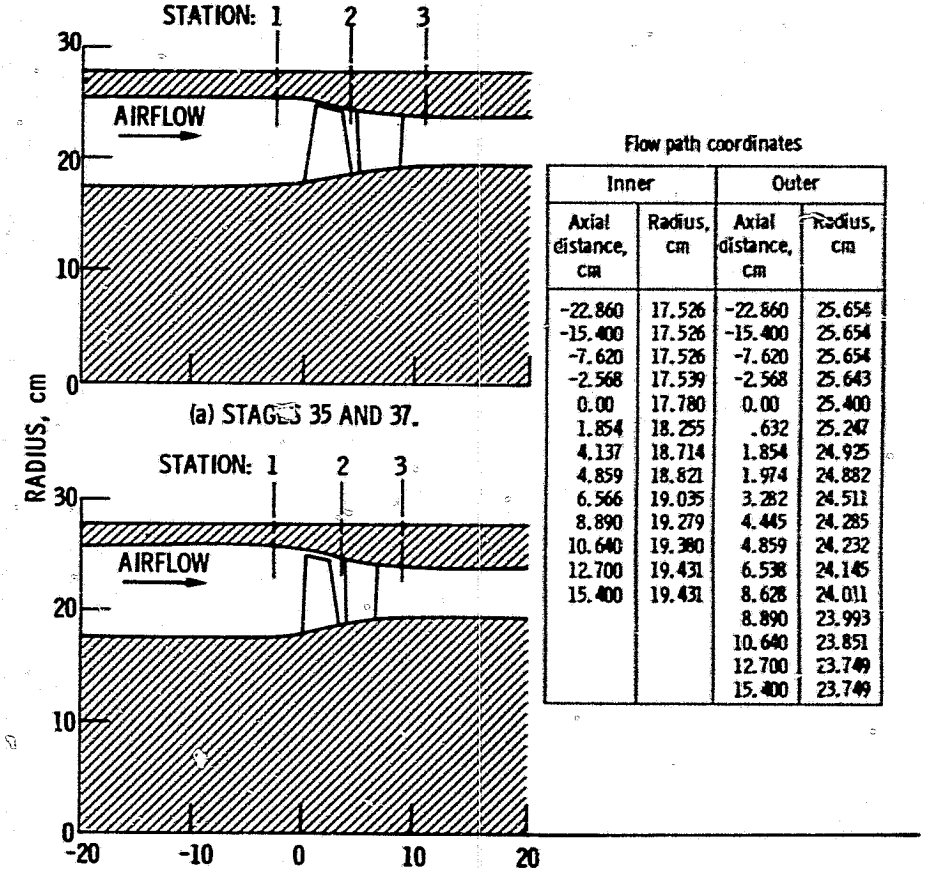

Flow path coordinates

Inner		Outer	
Axial distance, cm	Radius, cm	Axial distance, cm	Radius, cm
-22.860	17.526	-22.860	25.654
-15.400	17.526	-15.400	25.654
-7.620	17.526	-7.620	25.654
-2.568	17.539	-2.568	25.643
0.00	17.780	0.00	25.400
1.854	18.255	.632	25.247
4.137	18.714	1.854	24.925
4.859	18.821	1.974	24.882
6.566	19.035	3.282	24.511
8.890	19.279	4.445	24.285
10.640	19.380	4.859	24.232
12.700	19.431	6.538	24.145
15.400	19.431	8.628	24.011
		8.890	23.993
		10.640	23.851
		12.700	23.749
		15.400	23.749

Figure 2. - Flow path geometry.

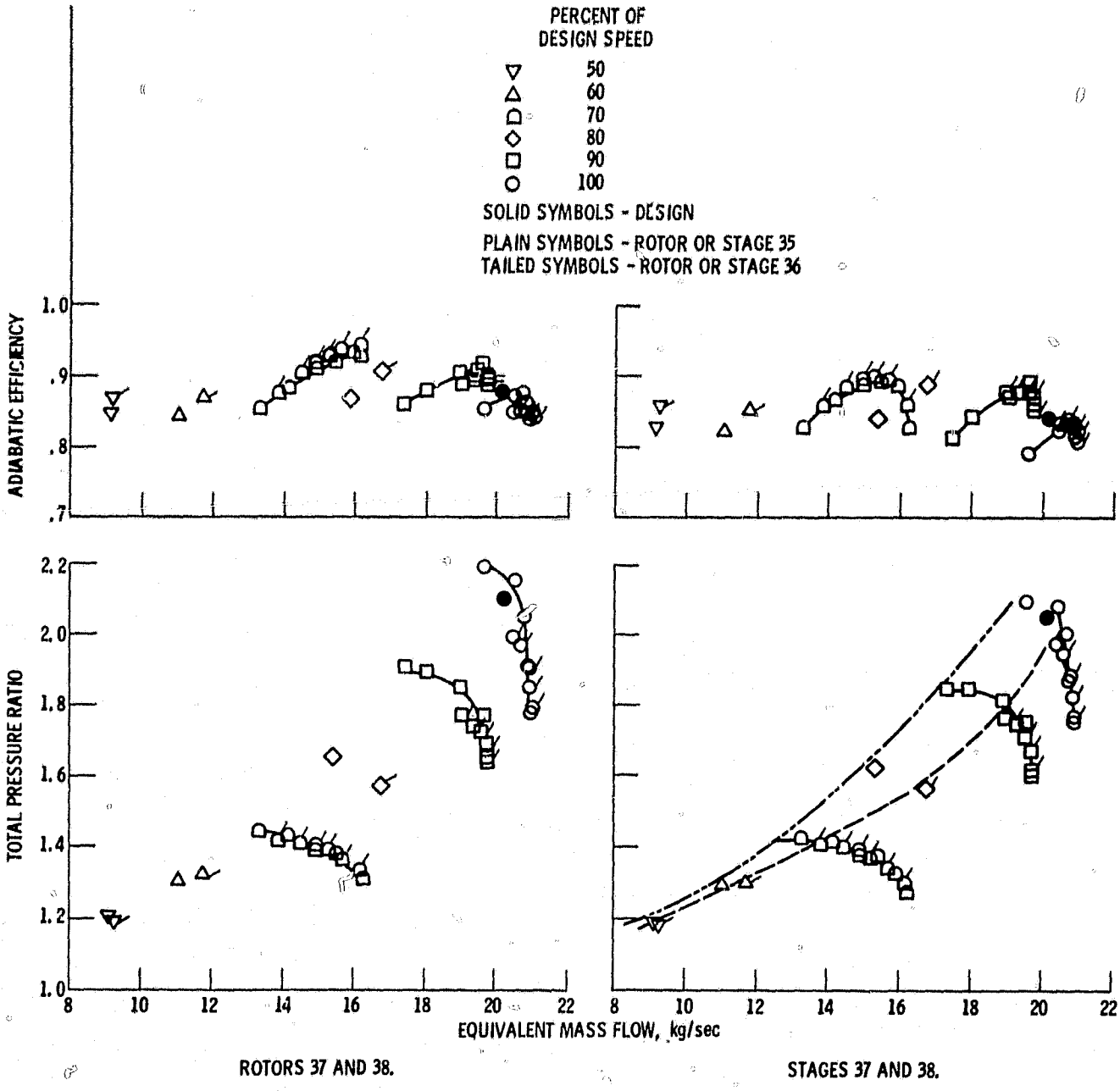

(a) DESIGN STAGE PRESSURE RATIO OF 2.05.

Figure 3. - Effects of blade aspect ratio on overall performance.

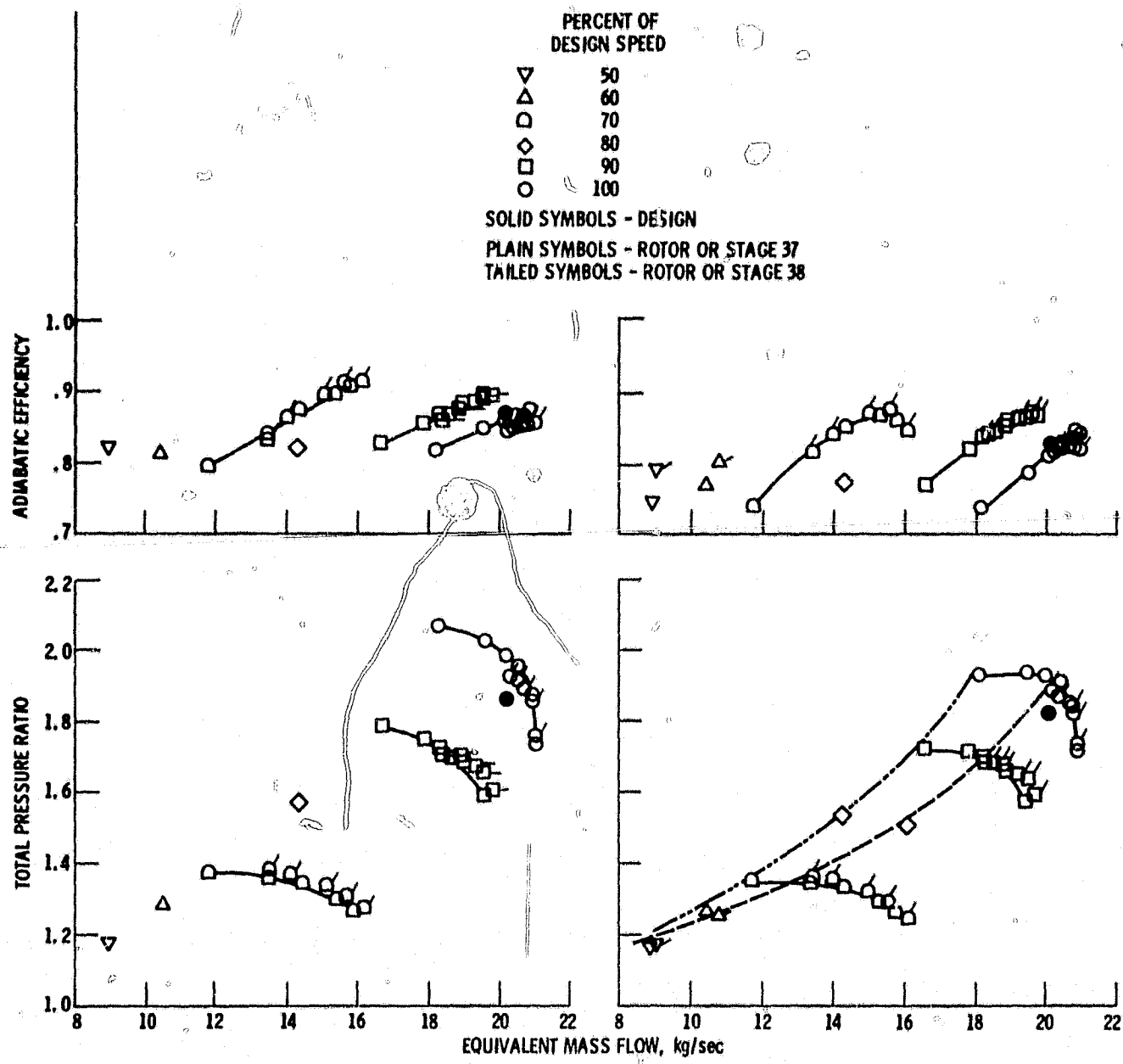

(b) DESIGN STAGE PRESSURE RATIO OF 1.82.

Figure 3. - Concluded.

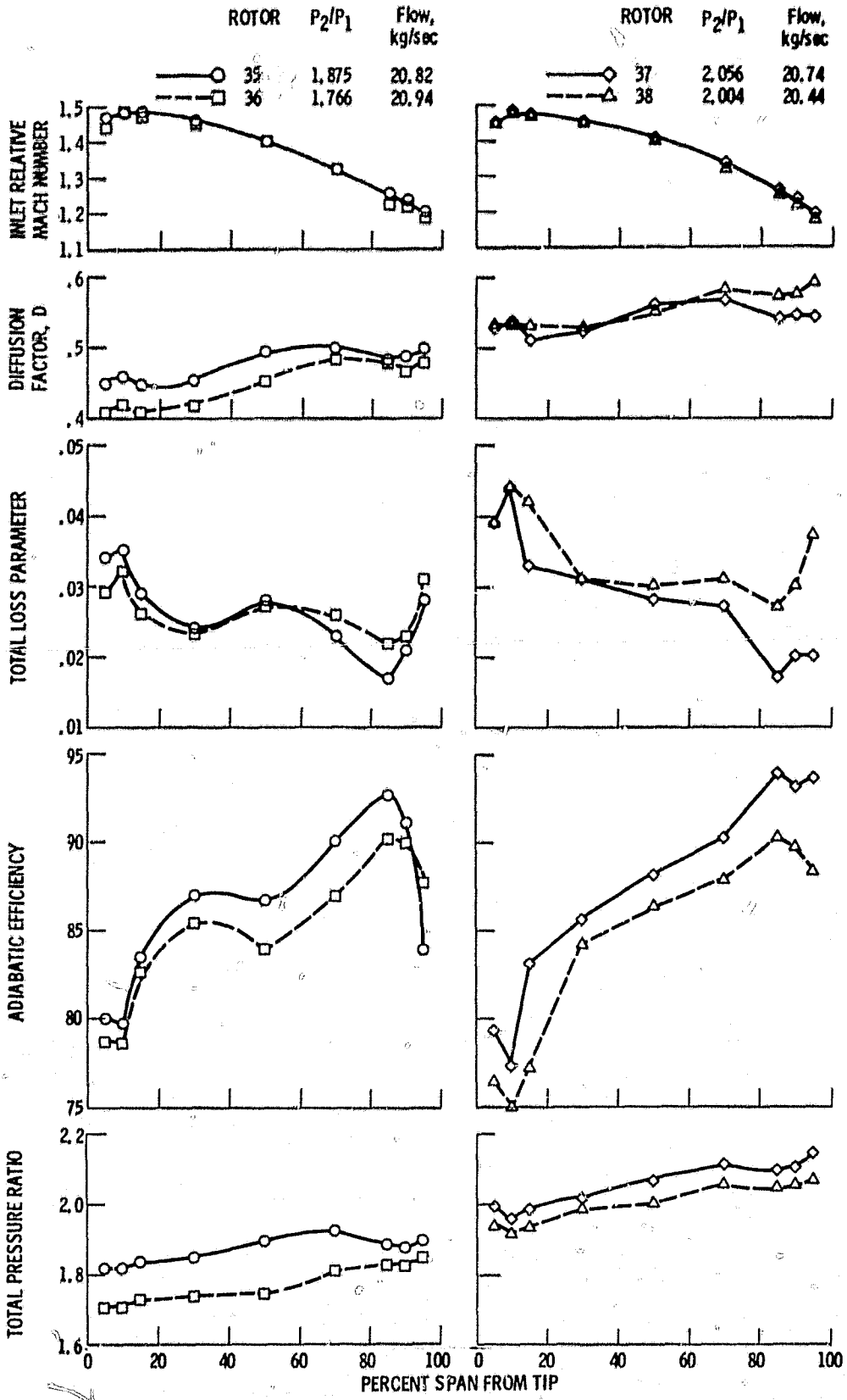

(a) DESIGN STAGE PRESSURE RATIO OF 1.82. (b) DESIGN STAGE PRESSURE RATIO OF 2.05.

Figure 4. - Radial distribution of performance parameters.

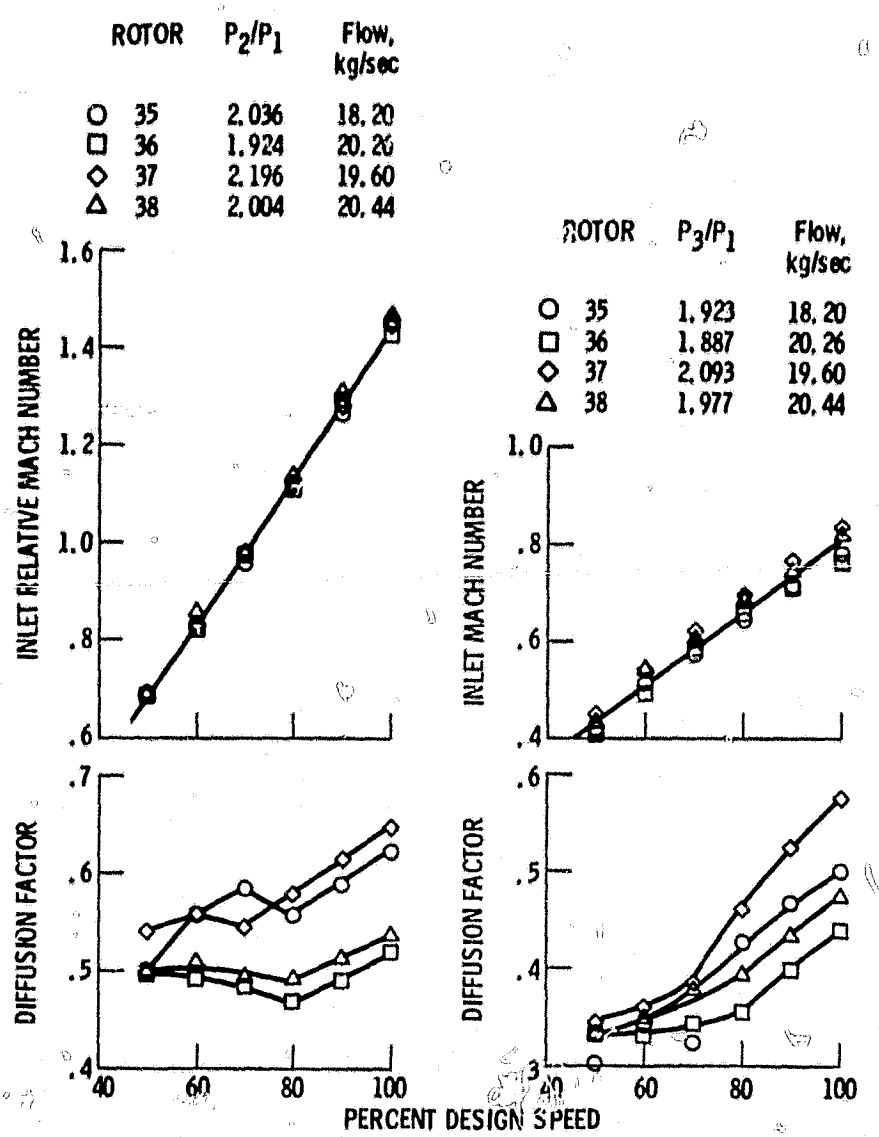

(a) ROTOR TIP (10% SPAN). (b) STATOR HUB (90% SPAN).

Figure 5. - Diffusion factor and inlet Mach numbers at near-stall conditions.

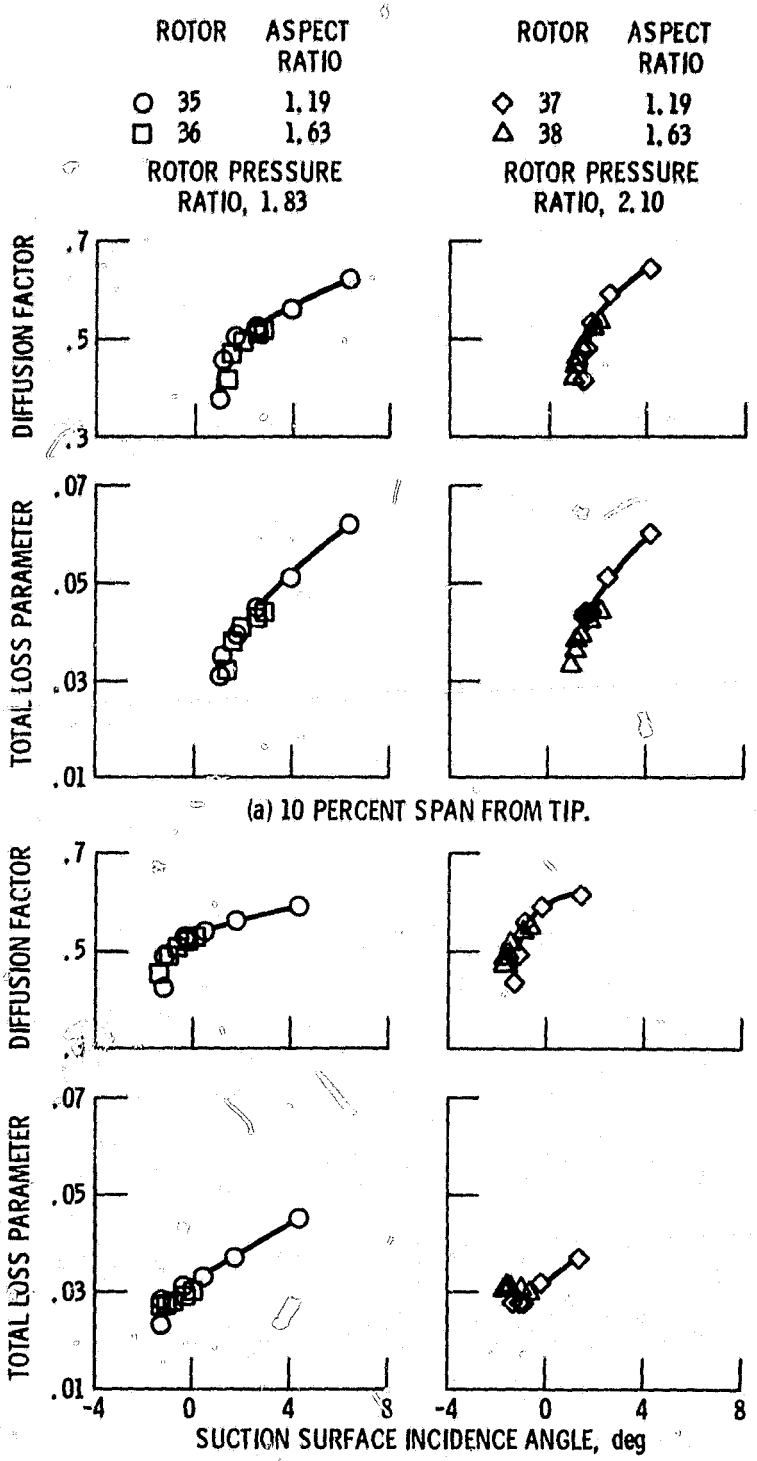

(a) 10 PERCENT SPAN FROM TIP.

(b) 50 PERCENT SPAN FROM TIP.

Figure 6. - Effects of blade aspect ratio on rotor blade element performance parameters.

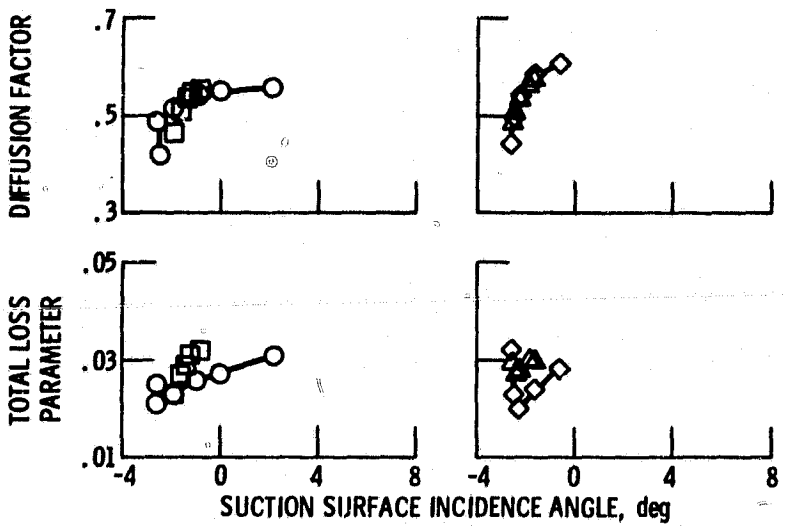

(c) 90 PERCENT SPAN FROM TIP.

Figure 6. - Concluded.

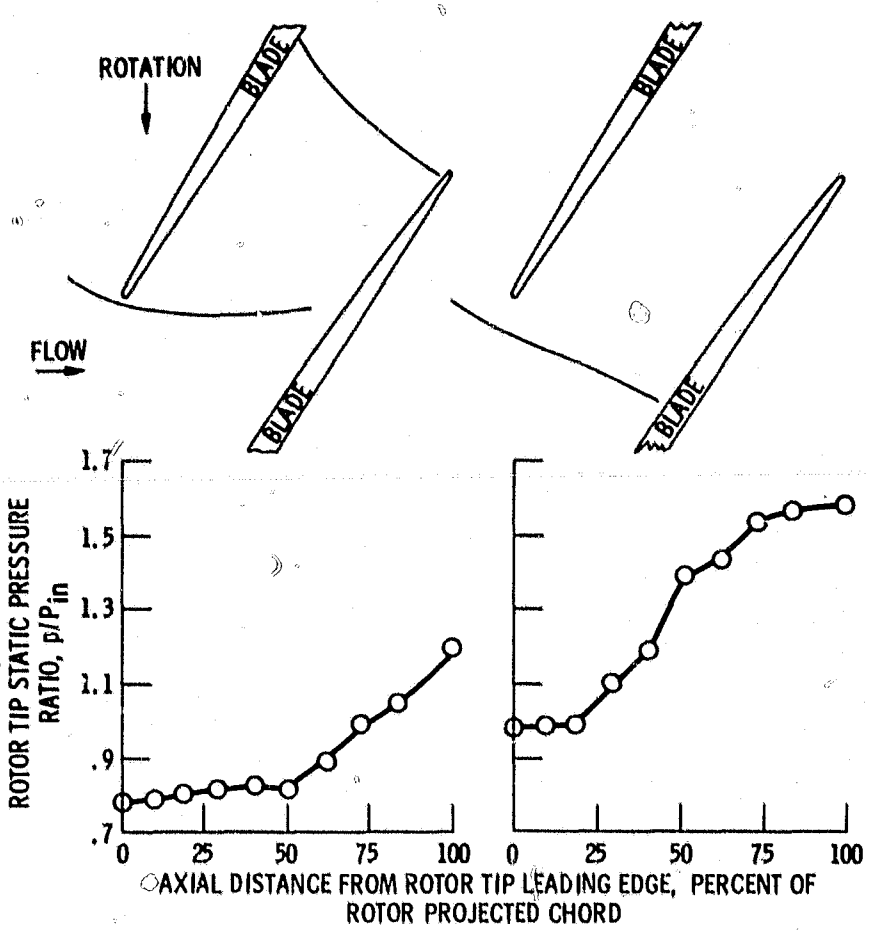

(a) NEAR CHOKE (HIGH FLOW). (b) NEAR STALL (LOW FLOW).

Figure 7. - Axial distributions of rotor tip static pressures and rotor shock patterns; rotor 33, design speed.

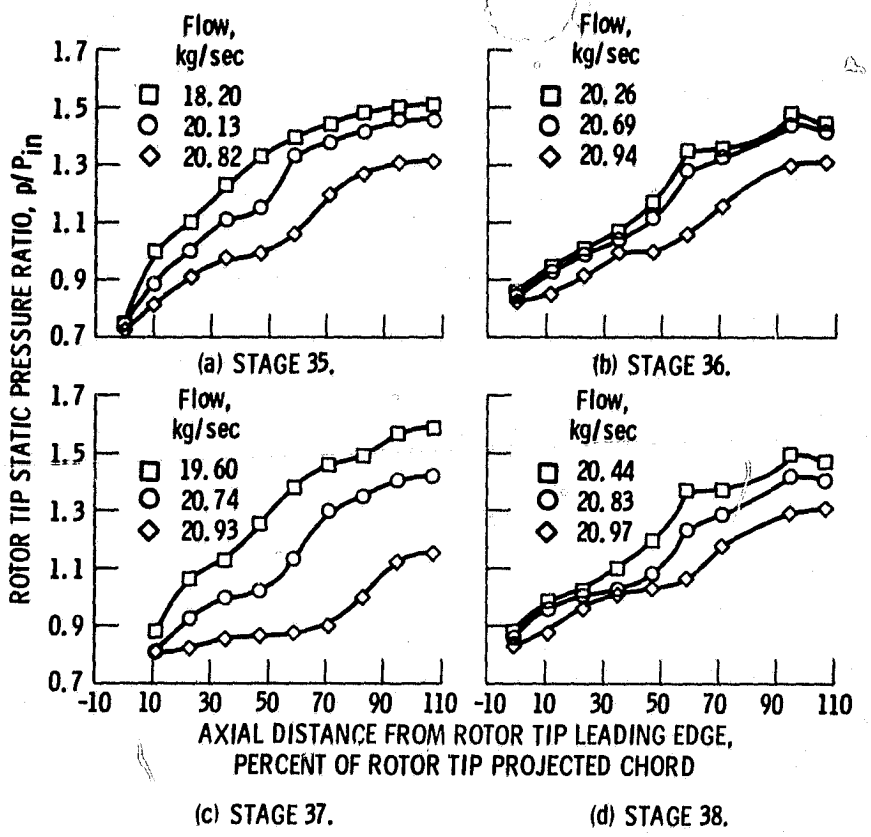

Figure 8. - Axial distribution of rotor tip static pressures, design speed.

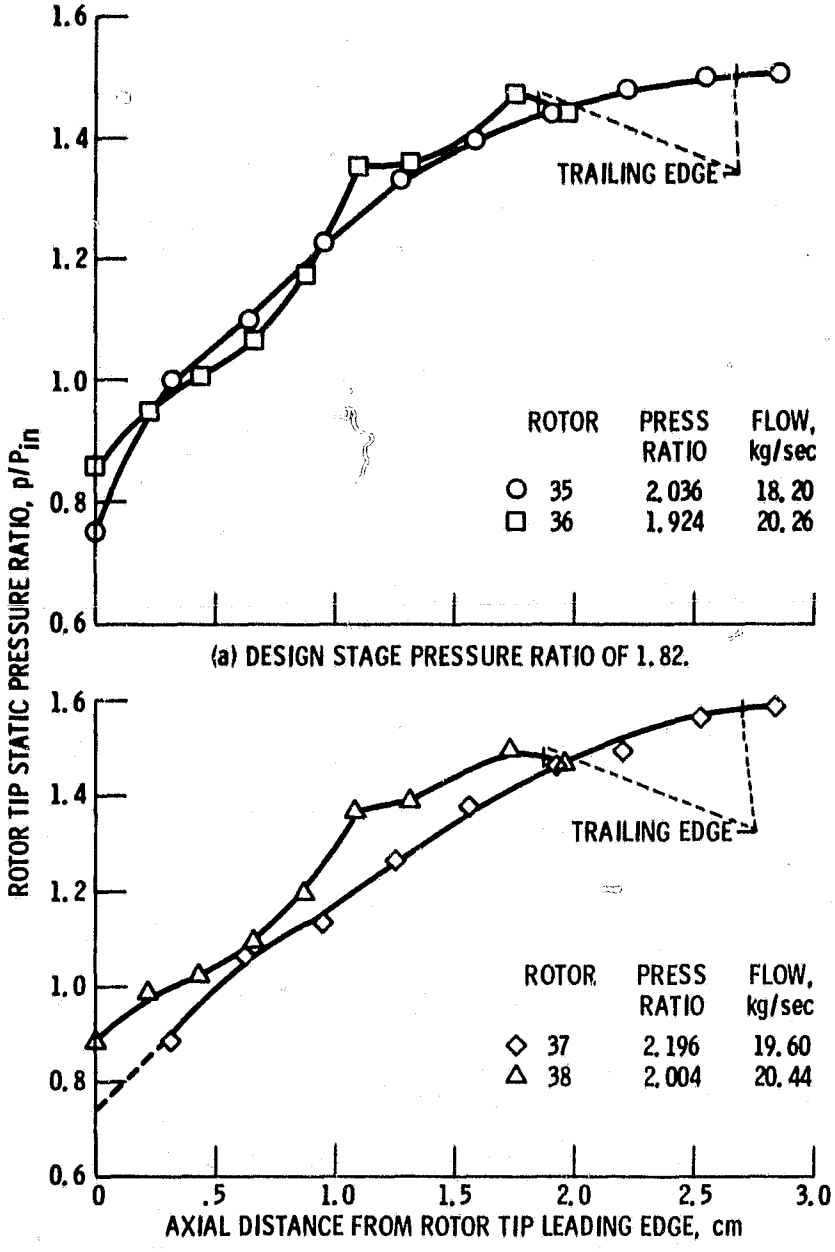

Figure 9. - Axial distribution of rotor tip static pressure, near stall condition design speed.